Journal of Nuclear Materials 398 (2010) 180–188

Contents lists available at ScienceDirect

Journal of Nuclear Materials

journal homepage: www.elsevier.com/locate/jnucmat

Preliminary evaluation of cavitation–erosion resistance of Ti-alloys in mercury for the Spallation Neutron Source

S.J. Pawel *, L.K. Mansur

Materials Science and Technology Division, Oak Ridge National Laboratory, 1 Bethel Valley Road, Oak Ridge, TN 37831-6156, USA

A B S T R A C T

A number of Ti-based alloys in both the mill-annealed and 20% cold-worked conditions were subjected to sonication conditions in Hg using a vibratory horn to assess relative cavitation–erosion resistance. Weight loss as a function of exposure time decreased monotonically with increasing hardness for all alloys/conditions examined, with Ti–6Al–4V (Grade 5) and Ti–6Al–2Sn–4Zr–2Mo yielding the best resistance to cavitation–erosion as evidenced by low weight losses and little or no tendency to form pits on the exposed surface. Unalloyed Ti (Grade 4) and Ti–0.12Pd (Grade 7) exhibited greater weight losses by a factor of about two and about five, respectively, with Ti–0.12Pd particularly prone to pitting development. The mean erosion rates of the best two Ti-alloys examined were about a factor of three higher than identically tested 316LN stainless steel following a low temperature carburizing treatment, but this difference is considered minor given that the rate for both materials is very low/manageable and represents a through-thickness property for the Ti-alloys. A nitriding surface treatment was also evaluated as a potential method to further increase the cavitation–erosion resistance of these alloys in Hg, but the selected treatment proved largely ineffective as measured by rapid weight loss. Recommendations for further work to evaluate the efficacy of Ti-based alloys for use in high-powered targets for the Spallation Neutron Source are given.

Published by Elsevier B.V.

1. Introduction

The Spallation Neutron Source (SNS) generates neutrons via interaction of a pulsed (60 Hz) high energy (1.0 GeV) proton beam with the liquid Hg target. The duration of each pulse is very short (<1 μs) and the temperature rise of the affected volume is modest (~10 °C), but the extreme local heating rate (on the order of 10^7 °C/s) is expected to give rise to a thermal-shock induced pressure wave. When the compression wave reaches a boundary – e.g., a container surface – it will be reflected back with a change of phase. The resulting rarefaction wave will expose Hg to transient negative pressures that are anticipated [1–3] to be sufficient to generate small cavitation bubbles/voids in nominal purity Hg. When the bubbles collapse – in principle with each proton pulse cycle – some of the energy is released as a jetting action of the liquid at extreme velocity, which is capable of causing localized cavitation–erosion damage of the container surfaces.

Type 316LN stainless steel was selected as the prime candidate target containment material [4] for the SNS based on a favorable combination of factors, including good compatibility with Hg up to moderate temperatures, well-characterized behavior in a neutron radiation environment indicating relatively gradual embrittlement with increasing radiation dose, and the absence of a ductile–brittle transition. At the time of this material selection, however, the severity of potential cavitation damage in Hg as a result of pressure pulse phenomena was largely unknown. Initial experiments and in-beam exposures designed to assess the potential for pitting as a result of cavitation damage in 316LN [5–7] revealed an array of irregular but roughly circular pits (order of a few μm deep, diameter somewhat greater) in numbers consistent with the number of total cavitation pulses in the exposure. Of particular concern was the concept that linear extrapolation of the cavitation damage (particularly pit depth) observed in the limited pulse (10–1000) exposures to anticipated target service lifetimes of >100 million pulses suggested the integrity of the target containment might be prematurely threatened by significant erosion or through-wall pits.

Susceptibility to pitting and erosion of stainless steel in Hg under cavitation conditions has been further demonstrated using a variety of laboratory based tests, including a split Hopkinson pressure bar (SHPB) apparatus [8] and a "drop test" variation [9], a vibratory horn [10–13], and a magnetically driven device [14] termed MIMTM. While it is difficult to compare the severity/intensity of cavitation conditions among these different techniques or with actual conditions in an SNS target, it is widely accepted that any one of these techniques permits a relative comparison of cavitation–erosion resistance as a function of material variables, such

* Corresponding author. Tel.: +1 865 574 5138; fax: +1 865 241 0215.
E-mail address: pawelsj@ornl.gov (S.J. Pawel).

0022-3115/$ - see front matter Published by Elsevier B.V.
doi:10.1016/j.jnucmat.2009.10.030

as thermal–mechanical treatment and/or surface modification. Among other results, vibratory horn tests have indicated [15] and in-beam tests have confirmed [9] that the cavitation–erosion resistance of annealed 316/316LN stainless steel can be substantially improved via cold-working or subjecting the material to a low temperature carburizing treatment.

While the improvement in cavitation–erosion resistance of 316LN with low temperature carburizing is encouraging as a method to potentially prolong target container life, additional vibratory horn testing suggests that eventually, under extended cavitation bombardment, the protection afforded by a surface treatment will be significantly reduced or eliminated [16] leaving essentially untreated base material with poor resistance exposed to aggressive cavitation conditions. This is an inherent problem for protection based on a near-surface (essentially external) condition rather than a through-thickness property of merit. Further, such a surface treatment is potentially susceptible to local flaws (for example, carburizing does not afford protection at points where inclusions intersect the exposed surface), and thus utilizing surface treatment as a protection scheme retains some risk for localized failure. Given that the SNS eventually hopes to implement a power upgrade (cavitation damage is considered to scale roughly as input beam power raised to the fourth power [9]), material and treatment combinations with even better cavitation–erosion resistance than surface-treated stainless steels are of interest.

Titanium alloys potentially represent an improved structural material for future liquid metal spallation target containers in general and proton beam windows in particular with respect to resistance to cavitation–erosion effects. The primary characteristics of interest include higher strength, a lower coefficient of thermal expansion, and a lower modulus of elasticity compared to stainless steels. Together, these attributes could result in reduced thermal stresses for an operating target. In addition, the considerably higher strength of Ti-alloys compared to stainless steels corresponds to potentially thinner beam windows, further reducing thermal stresses (lower thermal energy deposition) and improving heat transfer. Of more minor significance, the lower density of Ti-alloys corresponds to a greater neutron yield, as a greater fraction of the incident proton beam is able to interact with the Hg target rather than being parasitically scattered by the window material. Of specific interest to this study is that the higher strength/hardness of Ti-alloys (compared to 316LN stainless steel) may correlate to superior resistance to cavitation damage in Hg.

Ti–6Al–4V is one of a handful of commercially available titanium alloys. It is potentially an appropriate selection because it is readily available, there is extensive industry experience with fabrication, it has good strength at low to moderate temperatures, and it has well-characterized mechanical properties in a non-irradiation environment. It is a so-called $\alpha + \beta$ alloy, meaning that it is a phase mixture consisting of α (hcp crystal structure) and discontinuous β (bcc crystal structure) grains. The α phase is predominant, typically comprising about 80–90% of the material. The fractional phase distribution is strongly affected by heat treatment, and heat treatment is a powerful method of manipulating the properties of the alloy over broad ranges. The latter advantage contributes to the popularity of $\alpha + \beta$ alloys, because it allows relatively easy fabrication followed by optimization of properties via heat treatment after fabrication. A wide variety of microstructures can be produced for the same chemical composition, giving a method for tailoring the alloy to particular applications.

An initial assessment of titanium alloys with respect to irradiation performance for Spallation conditions [17] found that very little experimental data was available. However, based on the limited data accumulated under irradiations that did not represent spallation environments, titanium alloys could not be ruled out for this type of service and did appear to retain sufficient properties at low doses to merit consideration for Spallation target applications. It was recommended to proceed with a sequence of cavitation–erosion and compatibility testing to determine whether the effort and expense of more thorough testing for irradiation response relevant to Spallation sources would be justified.

The purpose of the present investigation is to use a standard screening test (vibratory horn) to compare the Hg cavitation damage resistance of Ti-alloys – principally Ti–6Al–4V – with previously examined 316LN stainless steel. Should the cavitation resistance be promising in comparison to that observed for 316LN and its variants, then further effort would be required to assess the radiation response characteristics of Ti-alloys in the SNS spectrum, to assess potential advantages associated with potential "reduced activation" compared to stainless steels, and to confirm expected good compatibility with Hg and oxidation resistance at SNS service temperatures.

2. Experimental procedure

Test specimens for cavitation–erosion testing were fabricated from material purchased from a commercial supplier. Alloys examined in the investigation included α-alloys Grade 4 (unalloyed Ti) and Grade 7 (Ti–0.2%Pd), the $\alpha + \beta$ alloy Grade 5 (Ti–6Al–4V), and the near-α alloy Ti-6–2–4–2 (Ti–6Al–2Sn–4Zr–2Mo). Table 1 gives the composition and room temperature mechanical properties of the supplied stock as reported on the material certifications for each material.

Microstructures of the as-received (mill-annealed) Ti–6Al–4V and unalloyed Ti appear in Figs. 1 and 2, respectively. These microstructures represent the alpha + beta and single phase alpha structures observed on the test face orientation of the nominal as-purchased material.

In addition to testing specimens in the as-received (mill-annealed) condition, specimens of each alloy were also examined following 20% cold reduction by swaging or rolling. In the case of the Ti–6Al–4V material, specimens cold-reduced 40% were also included (rod 2 in both cases). Specimens of Ti–6Al–4V (rod 1) were also examined following laboratory aging (540 °C, 1 h). To compare with specimens machined after mill-annealing, some Ti–6Al–4V specimens were prepared by machining mill-annealed specimens and subsequently laboratory annealing (705 °C, 1 h) to examine the potential effect of surface residual stresses due to machining. Specimens of each of the four different mill-annealed Ti-alloys were subjected to a nitriding treatment (975 °C, 24 h, in flowing $96\%N_2$–$4\%H_2$) selected primarily due to its relative efficacy as a method to deposit nitride coatings on Ti-bearing alloys for use in fuel cell applications [18], and a specimen of each alloy was also tested after removal of the nitride layer to distinguish any effect of the heat treatment time/temperature associated with the nitriding treatment.

Details of the test button size/shape have been described previously [13]. All specimens were machined at a local fabrication shop using the same drawing and specifications used to prepare specimens for all previous cavitation tests in this series and were identical to each other – including an average surface roughness of about 0.8 μm (corresponding to 32 RMS, or 32×10^{-6} in.) on the as-machined test face – with two minor exceptions. One is that the threaded shank on the Ti specimens was not drilled out as it was on stainless steel specimens to reduce specimen weight. Secondly, because the Ti-alloys examined here have a density only about half (~4.4 vs. 8.0 g/cm^3) of the 316LN stainless steel, the specimen head thickness for the Ti-alloys (7.42 mm) was chosen to be somewhat greater than for the stainless steel specimens (3.94 mm) in order to maintain the same specimen mass (8 g) on the end of the vibratory horn for these tests. In a limited number

Table 1
Composition and room temperature mechanical properties reported on mill certification documents for the specimen materials used in this investigation. In each case, the as-received materials were reported to be in the annealed condition.

Element (wt%)	Grade 4 rod	Grade 7 plate	Grade 5 (rod 1)	Grade 5 (rod 2)	Ti–6–2–4–2 plate
C	0.010	0.010	0.004	0.011	0.010
O	0.290	0.130	0.16	0.17	0.132
N	0.003	0.006	0.004	0.004	0.005
H	0.0036	0.0030	0.0009	0.0044	0.0047
Fe	0.160	0.120	0.05	0.18	0.090
Pd		0.120			
Al			6.08	6.20	6.13
V			3.97	4.10	
Si					0.080
Sn					1.95
Mo					1.97
Zr					3.93
Ti	Balance	Balance	Balance	Balance	Balance
Ult. tensile strength (MPa)	679.8	479.2	1054.2	974.9	985.9
Yield strength (MPa)	541.2	348.2	955.6	887.4	944.6
Reduction in area (%)	55.7	60.0	51.0	50.0	25.5

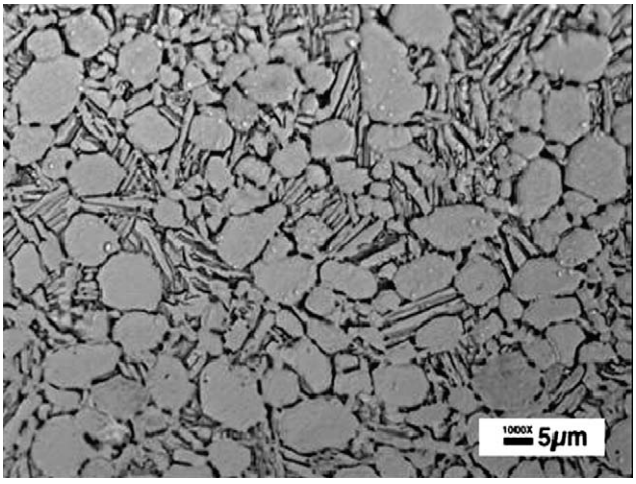

Fig. 1. Microstructure of the as-received (mill-annealed) Ti–6Al–4V (rod 1) material. The dual phase structure is predominantly alpha (light phase) with smaller amounts of beta (dark). Etched lightly with $85H_2O + 5HNO_3 + 10HF$.

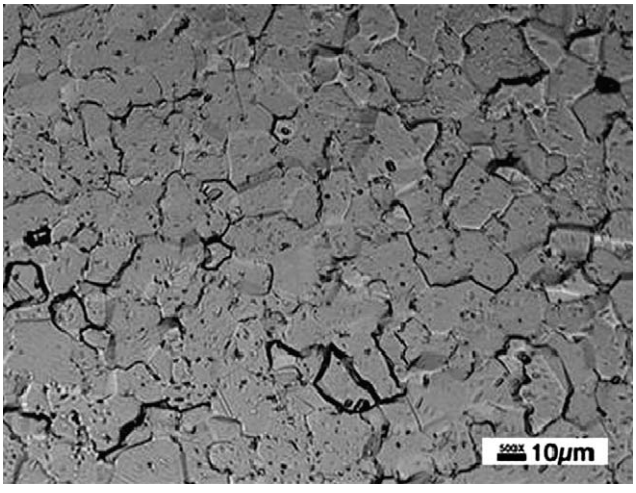

Fig. 2. Microstructure of the as-received (mill-annealed) unalloyed Ti material. The structure is essentially single phase alpha with relatively large grains. Etched lightly with $85H_2O + 5HNO_3 + 10HF$.

of cases, for the express purpose of examining specimen mass as a potential test variable, a few Ti–6Al–4V (rod 1) specimens were also fabricated with the lesser head dimension (3.94 mm, corresponding to a 5 g specimen weight).

All Ti-alloy specimens machined from rod were oriented such that the test face was perpendicular to the rod axis. Most specimens machined from plate were oriented such that the test face was perpendicular to the plate surface; however, a small number of specimens were prepared with a test face orientation parallel to the plate surface to permit ready assessment of orientation as a potential variable for the cavitation results.

Cavitation–erosion tests were performed using a titanium vibratory horn and the general test methodology described in ASTM G-32 [19]. Each test button had a surface area of 180 mm^2 exposed to cavitation conditions and was attached to the horn via a threaded shank. In all cases, the horn tip oscillated at a fixed frequency of 20 kHz and was set to generate a peak-to-peak vibrational amplitude of 25 μm. All tests were conducted in a jacketed stainless steel container (about 10 cm inside diameter), which permitted temperature control of the Hg at 25–26 °C during cavitation experiments via circulation of a water/glycol mixture from a constant temperature bath. The test specimen surface was immersed about 2 mm below the surface of the Hg (total pool depth about 11 cm) in the center of the container. Approximately one liter of high purity Hg was contained within the jacketed vessel and the same Hg was used for all experiments. Periodically, cheesecloth was used to skim the Hg surface and remove floating oxide and/or test debris.

Following exposure, test specimens were ultrasonically cleaned sequentially in (1) an aqueous solution containing thiosulfates and other dissolved sulfur species to chemically bind residual Hg, (2) distilled water, and (3) acetone, followed by forced air drying in each case. Specimens were then weighed and subsequently examined with an optical microscope to assess the average cavitation–erosion surface profile and to assess pitting. The profile determination was performed with the calibrated fine focus feature of the optical microscope. Each division on the fine focus knob corresponds to a one-micron vertical movement of the microscope stage, so by sequentially focusing first on the relative high point and then on the low point within a field of view, the depth of surface relief can be estimated. Typically, the average profile, or nominal surface roughness, was determined from measurements at 400x magnification on seven random – but regularly spaced – locations across the test surface. Observations of areas with profile significantly different than the average were noted as appropriate. Selected specimens were also sectioned for metallographic assessment of the surface profile and microstructural effects, and microhardness (Vickers) profiles across the surface layer into the

substrate were obtained on a limited number of the polished cross-sections.

3. Results and discussion

3.1. Specimen composition and treatment

Weight loss test results for Ti-alloys that did not receive a surface treatment are compared in Fig. 3 as a function of specimen hardness resulting from the various treatment/conditions examined. In this instance, the weight loss value reported is for 8 g specimens sonicated for 6 h. To aid in identification of the individual specimen conditions, Table 2 gives the hardness of each specimen alloy/condition included in Fig. 3. Although only the total weight loss in 6 h in given in Fig. 3, it was observed that the weight loss rate per hour for each alloy was remarkably constant over this duration of testing.

The results indicated in Fig. 3 are consistent with the general trend that cavitation–erosion resistance increases with hardness, although it should be noted that such is not always the case [13]. Note that the hardness of the various Ti–6Al–4V specimens was not significantly influenced by treatment and, as a result, the cavitation–erosion performance among these is indistinguishable. In absolute terms, the Ti-alloy with the lowest weight loss was the 40% cold-worked Ti–6Al–4V, but the difference between this specific result and that for the other Ti–6Al–4V conditions appears to be within the scatter (typically 2–5%) of the measurement technique. Weight loss for unalloyed Ti and Ti–0.12Pd were somewhat higher – by factors of about two and five, respectively – than for Ti–6Al–4V. Weight loss for the Ti–6Al–2Sn–4Zr–2Mo alloy (examined only in the annealed condition) was only about 5–10% greater than observed for the various Ti–6Al–4V alloy conditions.

Table 3 records the relative surface roughness assessments for the Ti-alloys represented in Fig. 3. Note that following 6 h sonication, the Ti–6Al–4V materials and the Ti–6Al–2Sn–4Zr–2Mo alloy revealed a nominal peak-to-trough roughness of only 8–11 μm for all conditions examined – about twice the value of 4–6 μm noted for similarly sonicated 316LN after low temperature carburization. The nominal surface roughnesses for the unalloyed Ti and Ti–0.12Pd specimens were ~3 times and ~10 times greater, respectively, than observed for Ti–6Al–4V specimens. Also note that, with the exception of the relatively soft Ti–0.12Pd materials, the Ti-alloys appear relatively immune to pitting. The 316LN specimens sonicated in this fashion revealed variable degrees of susceptibility to pitting. The annealed 316LN material was very quickly and relatively deeply cratered across the surface. The 50% CW 316LN material also exhibited pits, but they tended to be much more shallow than observed for annealed material. The carburized material tended to be relatively immune to pitting, although isolated instances of deep pitting ascribed to inclusions intersecting the surface were not uncommon [15], and pitting susceptibility increased with extended sonication time [16] as the protective surface layer was eroded.

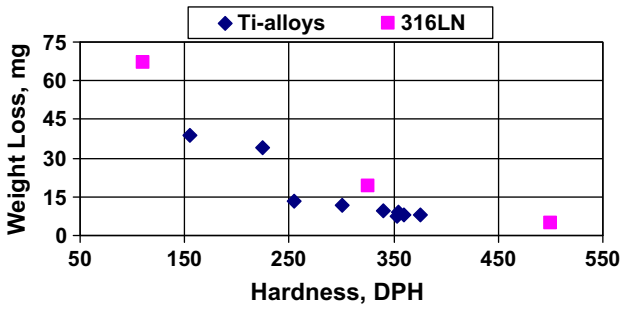

Fig. 3. Weight loss of Ti-alloys as a function of hardness following sonication for 6 h in Hg. In all cases, the weight loss result represents the average of at least two specimens. For comparison, equivalent test data for type 316LN stainless steel in several conditions is included, although the density difference between 316LN and Ti-alloys complicates direct comparison.

Fig. 4 compares the post-test appearance of the mill-annealed Ti–6Al–4V and Ti–0.12Pd specimens following 6 h sonication in Hg. At the modest magnification shown, the Ti–6Al–4V specimen is smooth and uniform – essentially indistinguishable from the unexposed condition. It is obvious, however, that the Ti–0.12Pd specimen has developed significant roughness in comparison.

Fig. 5 compares SEM images of the test surface of mill-annealed Ti–6Al–4V and Ti–0.12Pd specimens following 6 h sonication in Hg. This series of photographs depicts the relative profile/roughness development on the Ti–6Al–4V material (among the most resistant) compared to Ti–0.12Pd material (the least resistant). At the highest magnification, the similarities in the finest scale of damage on both specimen surfaces suggests that the mechanism of material loss – that is, fatigue-like behavior in which microcracks must be initiated and coalesce/propagate to effect material loss [20] – is very similar for these different materials. It would appear that the greater hardness of the Ti–6Al–4V material simply slows the rate of material loss by decreasing the rate of crack propagation or perhaps by shedding more cavitation energy elastically from the exposed surface.

Sonication time was extended up to 12 h (almost 1 billion strokes of the vibratory horn) for some of the mill-annealed Ti–6Al–4V specimens, and weight loss as a function of time is given in Fig. 6. Five total specimens are represented in Fig. 6; three are 5-g specimens (exposed 9–12 h) and two are 8-g specimens (exposed 6 h). Since the weight loss data (and surface roughness and pitting) were indistinguishable, it appears – as expected – that specimen mass does not significantly influence the magnitude of weight loss result in the cavitation test as performed here. As a curiosity, however, it was routinely observed that the energy required to operate the vibratory horn (as recorded by a kJ-counter on the control unit) was approximately three times greater per unit time for the larger specimen, and this appears to contribute to periodic performance issues for the horn (e.g., premature shutdown of the device during a timed exposure due to excessive energy requirement to vibrate the horn – this is considered a "safety" feature that prolongs the operating life of the device).

Based on the data in Fig. 6, the rate of weight loss with sonication time was essentially constant for mill-annealed Ti–6Al–4V with a value of approximately 1.25 mg/h. Using a density of 4.4 g/cm^3 and assuming relatively uniform attack (see Ti–6Al–4V results in Figs. 4 and 5), the weight loss rate for Ti–6Al–4V in Fig. 6 corresponds to a mean erosion rate of about 1.6 μm/h. Note that this value is consistent with the surface roughness estimate of 9 μm in 6 h sonication given in Table 3. In comparison, the "steady state" weight loss rate for the surface-carburized 316LN stainless steel was found to be about 0.7–0.8 mg/h [15,16], which – adjusting for density – corresponds to a mean erosion rate of about 0.52 μm/h. Although the sonication times were not similarly extended beyond 6 h for the other Ti-based materials in this study, all materials exhibited essentially constant weight loss rates that depended on alloy composition and treatment. Although the best Ti-alloys exhibited mean erosion rates about a factor of three higher than the surface-treated stainless steel, the results are considered very favorable for the Ti-alloys because the rate is very low and manageable (uniform and predictable) and represents a through-thickness property (unlike the that for the treated stainless steel). That is to say that the carburized layer on the stainless steel is very protective, but it slowly erodes during the vibratory horn exposures in mercury, and eventually fails thereby exposing a substrate that has relatively poor cavitation–erosion resistance.

Table 2
Average hardness values (measured in R_b and R_c, converted to DPH using standard hardness conversions derived for steel) for Ti-alloy specimens and 316LN stainless steel specimens exposed to cavitation testing in Hg. Average of three hardness measurements reported. The designation "CW" indicates cold-worked by the given percent.

Ti-alloy/condition	Hardness (DPH)	316LN condition	Hardness (DPH)
Ti–6Al–4V, annealed	375	Annealed	110
Ti–6Al–4V, aged	360	50% CW	325
Ti–6Al–4V, 20% CW	355	Carburized	500[a]
Ti–6Al–4V, 40% CW	355		
Ti–6Al–2Sn–4Zr–2Mo, annealed	340		
Unalloyed Ti, 20% CW	300		
Unalloyed Ti, annealed	255		
Ti–0.12Pd, 20% CW	225		
Ti–0.12Pd, annealed	155		

[a] Hardness measured at mid-thickness of the case layer.

Table 3
Average surface roughness values (seven measurements each specimen; results for two specimens averaged) and relative pitting tendency for Ti-alloy specimens sonicated 6 h in Hg. Surface indications are considered "pits" in this case when visible/distinct at 15x magnification.

Ti-alloy/condition	Nominal surface roughness (μm)	Relative pitting description
Ti–6Al–4V, annealed	9	None
Ti–6Al–4V, aged	11	Only one pit, 38 μm deep
Ti–6Al–4V, 20% CW	10	None
Ti–6Al–4V, 40% CW	8	Only one pit, 45 μm deep
Ti–6Al–2Sn–4Zr–2Mo, annealed	9	None
Unalloyed Ti, 20% CW	14	Only one pit, 23 μm deep
Unalloyed Ti, annealed	16	None
Ti–0.12Pd, 20% CW	93	Many; up to 150 μm deep
Ti–0.12Pd, annealed	95	Many; up to 170 μm deep

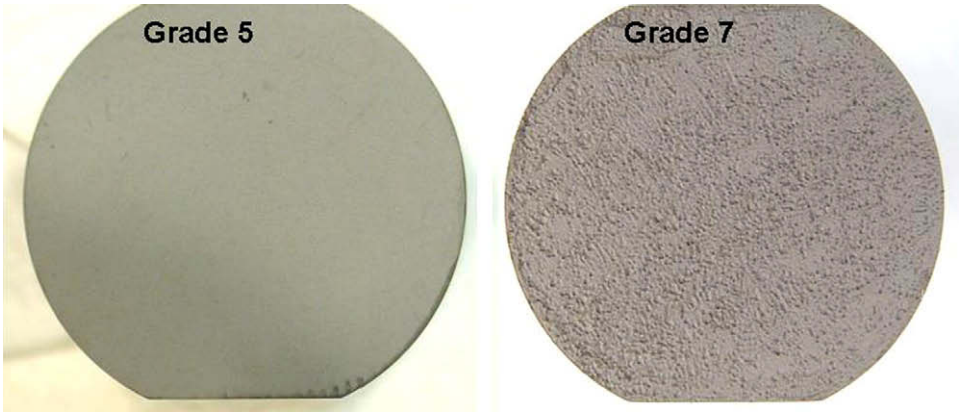

Fig. 4. Test surfaces of mill-annealed Ti–6Al–4V (Grade 5) and Ti–0.2%Pd (Grade 7) specimens following sonication in Hg for 6 h. For scale, the actual specimen diameter is 16 mm.

In contrast, the superior Ti-alloys are not dependent on a thin/temporary protective layer but on relatively good inherent resistance of the base material to cavitation.

3.2. Specimen orientation

Specimens of Ti–6Al–2Sn–4Zr–2Mo and Ti–0.12Pd were fabricated in two orientations from the mill-annealed starting plate material. Although insufficient replicates were examined to draw a firm conclusion, it appears that the specimens with a test face parallel to the original plate surface exhibited weight losses perhaps 10–20% less than for specimens with a test face perpendicular to the plate surface. However, the general post-test appearance and roughness of all the specimens followed the same basic pattern independent of specimen orientation.

3.3. Nitriding treatment

The nitriding treatment was observed to affect each alloy in a slightly different fashion. Ti–0.12Pd and unalloyed Ti gained the most weight from the treatment and turned a uniform dark golden brown on the surface, while Ti–6Al–4V (annealed and 20% CW conditions) and the Ti–6Al–2Sn–4Zr–2Mo alloy gained significantly less weight and turned a very light golden yellow color, suggesting that for this particular treatment, susceptibility to nitriding is at least somewhat sensitive to composition.

In addition, the microstructure of each alloy yielded changes consistent with differing amount of nitrogen uptake and variable response to the required thermal cycle. For example, representing the Ti–6Al–4V and Ti–6Al–2Sn–4Zr–2Mo materials, Fig. 7 shows the microstructure of the nitrided Ti–6Al–4V alloy in the 20%CW

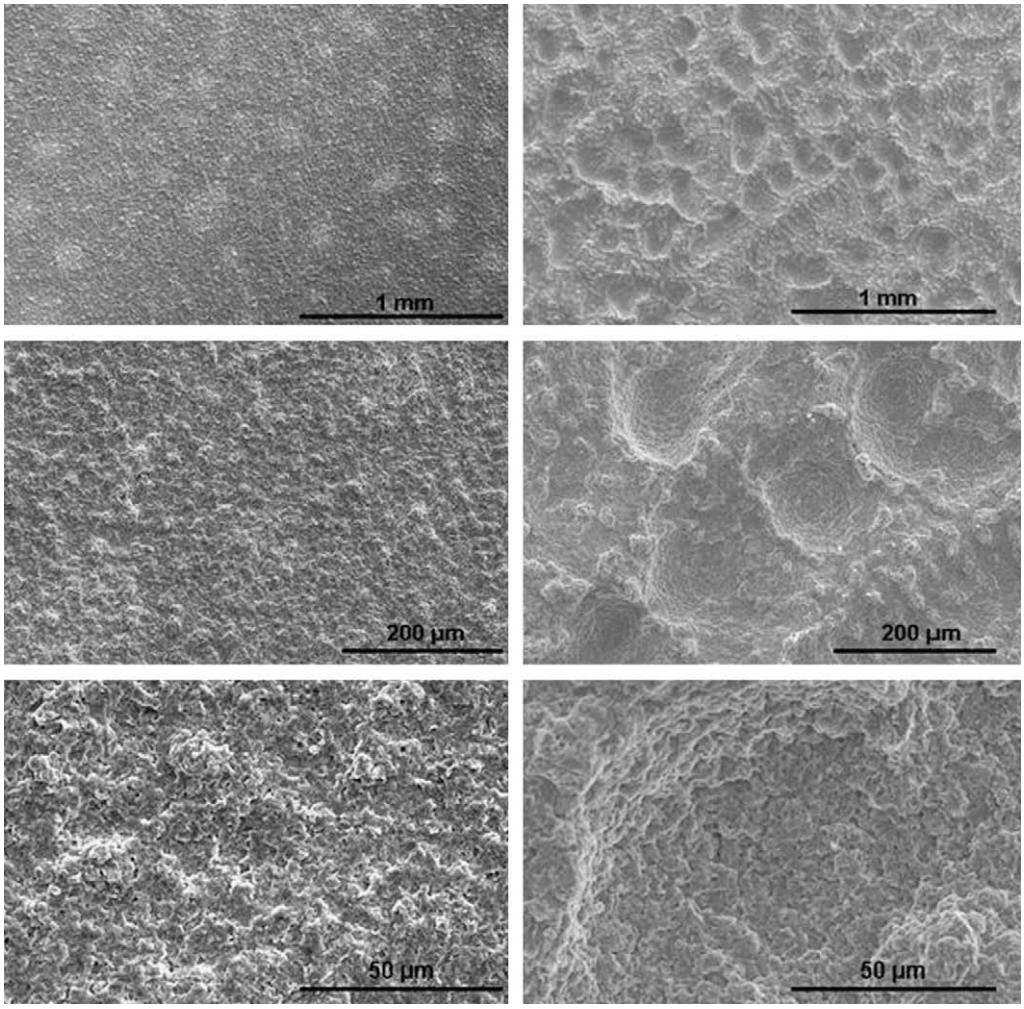

Fig. 5. SEM images of the test surface following 6 h sonication in Hg of: left column – a Ti–6Al–4V specimen, and right column – a Ti–0.12%Pd specimen.

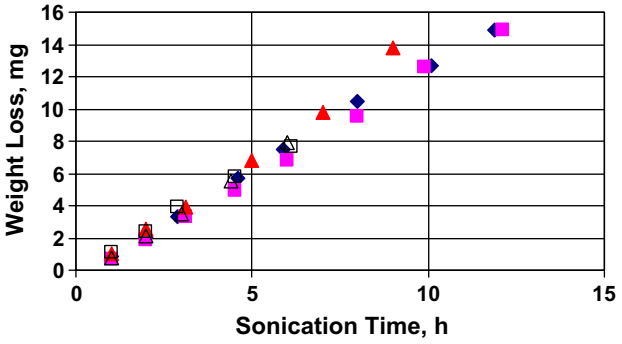

Fig. 6. Weight loss as a function of sonication time for Ti–6Al–4V in the mill-annealed condition. Five total specimens are represented (each by a different symbol), and mass loss is sufficiently similar among these that some data points are obscured by others on the plot.

condition. In the top portion of the figure (lower magnification), the bulk alloy structure resulting from the nitriding thermal treatment (24 h at 975 °C) can be seen to contain primarily acicular alpha phase, and the microhardness scan of this area indicated 350–400 DPH, or about the same as the mill-annealed hardness. Near (but distinctly below) the exposed surface of the specimen, there is a band about 200–225 μm thick that exhibits a mixed, or partially transformed, structure different than that of the bulk material due to variable degree of nitrogen penetration (but less at this position than nearer the surface). The alpha phase in this alloy is stabilized by nitrogen, and thus the extent of this band dominated by the alpha phase suggests the extent of penetration of nitrogen in quantities sufficient to cause the partial transformation. The microhardness of this band of mixed structure is in the range of 400–450 DPH, which is slightly harder than the bulk material; a step function change in hardness across the boundary between the bulk material and that partially transformed region was not observed. In the lower portion of Fig. 7 (higher magnification), the near-surface region can be resolved into (at least) two distinct components. The outermost layer, about 10–12 μm thick, has not been analytically identified but is likely to be TiN, which is commonly light golden brown. The TiN layer, which contains some evidence of structure, is too thin for reliable microhardness measurement, but it is likely to be quite hard compared to the other components of the structure. Slightly deeper into the specimen, just below the TiN layer, is a band about 25 μm wide which appears to have very little indication of structure in this photograph. Views in other locations around the specimen cross-section reveal what appear to be quite large/wide alpha grains – no other phase present – with boundaries essentially perpendicular to the specimen surface. As a trend, however, the grain boundaries in this band seem to resist demarcation by the etchant very well (perhaps encouraged by the high nitrogen content, which is widely considered to improve general and localized corrosion resistance of many

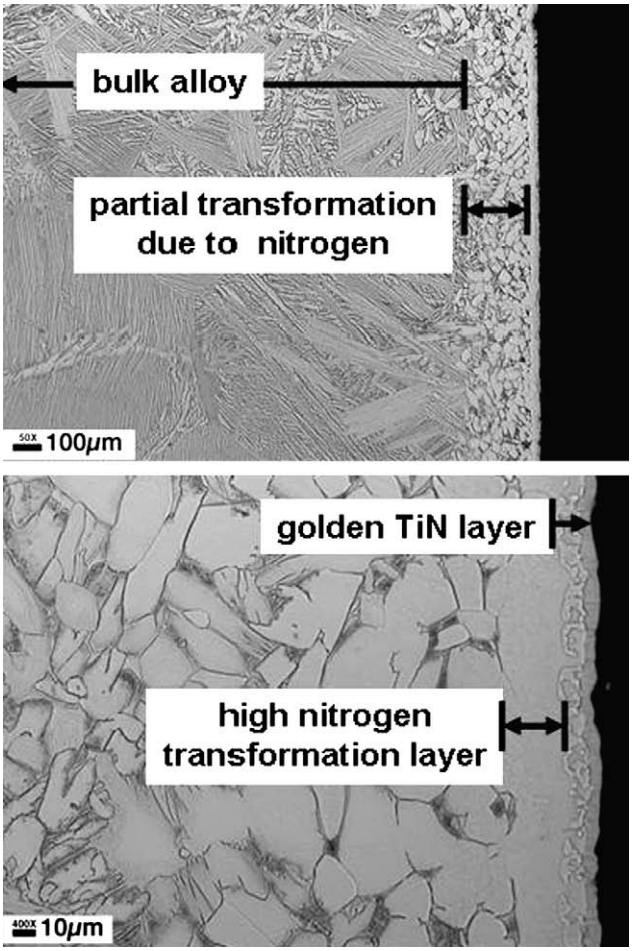

Fig. 7. Cross section of 20% cold-worked Ti–6Al–4V following nitriding. The views here were taken from the side of the specimen and represent an area not exposed to sonication. The specimen surface is at the right in each case (mounting epoxy is black); the top photograph (originally 50x) is an overview of the different structures present across the specimen thickness and the bottom photograph (originally 400x) resolves the different surface layers. Etched with $85H_2O - 5HNO_3 - 10HF$.

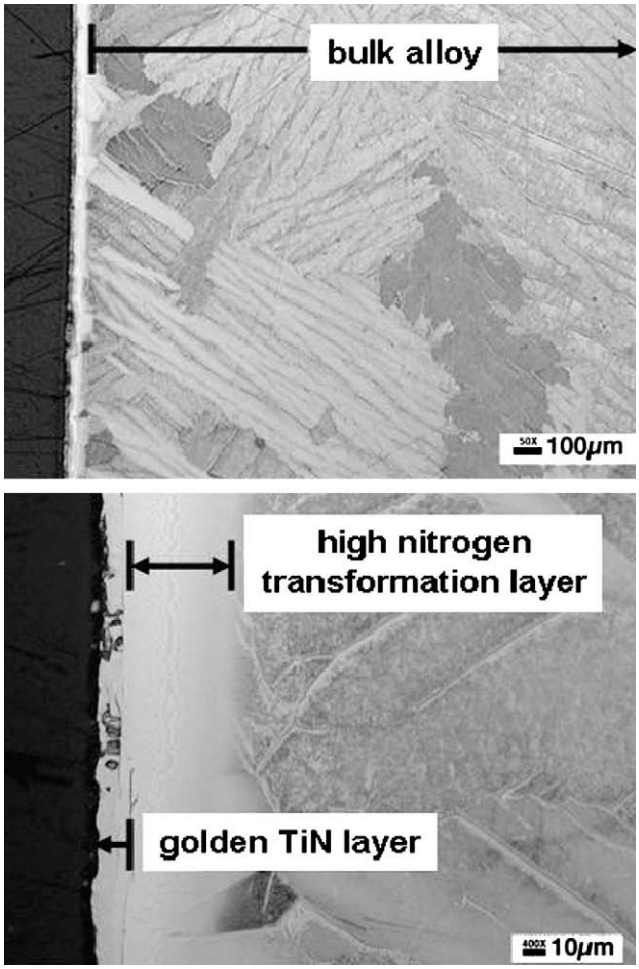

Fig. 8. Cross section of mill-annealed unalloyed Ti following nitriding. The views here were taken from the side of the specimen and represent an area not exposed to sonication. The specimen surface is at the left in each case (mounting epoxy is black); the top photograph (originally 50x) is an overview of the different structures present across the specimen thickness and the bottom photograph (originally 400x) resolves the different surface layers. Etched with $85H_2O - 5HNO_3 - 10HF$.

materials). In any case, the lattice strain resulting from a high level of nitrogen doping leads to substantially increased hardness; the maximum microhardness measured in this region was approximately 675 DPH.

Mill-annealed Ti–0.12Pd and unalloyed Ti specimens reacted somewhat differently to the nitriding treatment. Representing these alloys, Fig. 8 shows the structure of the nitrided unalloyed Ti material. The outermost surface layer of TiN is about 10 μm thick (similar for all alloys), and immediately adjacent/beneath the TiN is a high nitrogen layer approximately 45–55 μm thick. Similar to the Ti–6Al–4V alloy shown in Fig. 7, the region labeled "high nitrogen transformation layer" in Fig. 8 suggests some semblance of structure within a region that is largely resistant to the etchant. Microhardness within the high nitrogen layer was observed to range widely from about 1025 DPH nearest the TiN layer to about 650 DPH near the innermost position. Unlike the structure observed in Fig. 7, there is little or no mixed zone beneath the high nitrogen layer exhibiting a microstructure distinct from the remainder of the bulk material, and the microhardness of the reminder of the material thickness is relatively uniform and slightly harder than the mill-annealed material at 275–300 DPH.

Table 4 summarizes the observed microstructure zones and hardness values for all of the nitrided specimens. In all cases, data was gathered from the cross-section of specimens that were nitrided and subsequently sonicated for 3 h in Hg. Comparison of the structures/layers present on the specimen surface (exposed to sonication) and the side (not exposed to sonication) contributed to the assessment of the efficacy of the nitriding treatment.

The nitriding treatment was not effective for reducing cavitation–erosion damage in Hg in the vibratory horn screening test for any of the alloys under investigation. Representative results are shown in Fig. 9 for the Ti–6Al–4V alloy in a variety of conditions. The "open" data points represent material that was either not nitrided or had 500 μm removed (by light grinding; designated "ground" in the graph) from the test surface following nitriding to eliminate all microstructure zones with high nitrogen so as to expose only the base metal resulting from the nitriding thermal treatment to sonication conditions. The "closed" data points represent results for nitrided surfaces. It was observed in all cases that the TiN layer – light golden brown in this case for Ti–6Al–4V – was completely removed from the test surface in less than 10 min in the initial exposure period. (A limited number of tests were interrupted during the initial hour of sonication to make this observation.) The TiN layer is apparently sufficiently hard/brittle and/or poorly bonded to the substrate that only very brief sonication is sufficient to remove it from the surface. This is consistent with previous data for cavitation in Hg indicating hardness alone

Table 4
Nitriding characteristics exhibited by the Ti-based alloys under investigation. Microhardness scans performed with 100 g load on lightly etched cross-sections.

	Ti–6Al–4V annealed	Ti–6Al–4V 20% CW	Ti–6Al–2Sn–4Zr–2Mo annealed	Unalloyed Ti annealed	Ti–0.12Pd annealed
Normalized weight gain per unit area on nitriding[a]	1.2	1.0	1.1	1.5	1.6
TiN surface layer thickness (μm)	10–12	10–12	10–12	10	10
High nitrogen transformation zone thickness (μm)	30	25–30	20	45–55	38–50
High nitrogen transformation zone hardness (DPH)	550–725	525–675	650–700	650–1025	625–850
Partial transformation zone thickness (μm)	~250	200–225	~350	~None	~None
Partial transformation hardness (DPH)	400–450	400–450	475–500		
Base metal hardness after nitriding treatment (DPH)	350–375	350–375	375–425	275–300	250–275
Base metal hardness after mill-annealing (DPH)	375	355	340	255	155

[a] The entire coupon – not just the test face exposed to cavitation conditions – was nitrided in each case. The area of each test face was identical, but the total surface area varied somewhat among coupons due to variations in the head thickness as described in the Section 2. The total weight gain per unit area resulting from nitriding was normalized to the lowest value to readily display the differing tendency to react with nitrogen of each alloy type. For example, annealed Grade 7 gained 60% more weight than an equivalently treated 20% CW Grade 5.

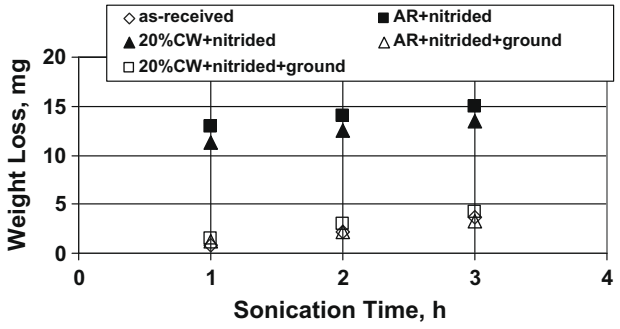

Fig. 9. Weight loss as a function of sonication time in Hg for Ti–6Al–4V specimens in a variety of conditions. Results given are for the average of two specimens. Notations include: AR = as-received/mill-annealed condition; 20%CW = cold-worked 20%.

is a poor predictor of cavitation–erosion resistance [13] and that coating integration/bonding with the substrate is critical [15].

It is curious, however, that the weight loss experienced by these nitrided specimens in the initial exposure period is considerably larger than would be predicted from consideration of the visual extent of damage. For example, the total mass gain associated with the nitriding process (made of up the visible golden surface phase, any precipitates, and all the dissolved nitrogen) is known for each specimen, and post-test metallography reveals that – except for the test surface – there are no apparent changes in the pre- and post-test appearance of the nitrided layers and substructure on any region of the specimen. As a first approximation, then, the expected weight change associated with the failure of the surface coating (corresponding to about 20% of the total specimen surface area, including test surface, cylindrical sides, and threads) might be expected to correspond to a similar fraction of the total weight gain associated with nitriding. However, 20% of the total mass gain associated with nitriding is considerably smaller (by a factor of 2–3) than the ~10 mg change shown in Fig. 9. The reason(s) for this unexpected result are not clear. The possibility of selective leaching of alloying elements by the Hg (particularly Al, which is known to interact aggressively with Hg under some circumstances) was considered but rejected because the same phenomena was observed for ALL the nitrided specimens, even for unalloyed Ti. A more subtle attack that leaches nitrogen remains a possibility, but such large mass changes in short times at room temperature make this seem unlikely. Since the nitriding effort was not considered successful, the details associated with this potential anomaly were not pursued, but further investigation is recommended if nitriding the Ti-alloys is considered for further development.

Following the considerable weight loss associated with rapid/complete removal of the TiN layer (and other unknown material as mentioned in the previous paragraph) from the test surface, however, the weight change as a function of sonication time was observed to return to a value approximating that of the untreated material. This is most readily seen by comparing the weight loss rate for the different conditions shown in Fig. 9, in which the apparent slope for each material condition is very similar for the time between 1 and 3 h sonication.

While not apparent from the level of detail in Fig. 9, the weight loss rate for the nitrided specimens (closed data points; testing the residual surface after the TiN layer was removed by sonication) falls in the range 0.95–1.05 mg/h (compare to 1.25 mg/h in Fig. 6 for mill-annealed Ti–6Al–4V not exposed to nitriding). It is suspected that this slight improvement in cavitation–erosion resistance (compared to the as-received/mill-annealed material) results from the relative hardness increase over the base material exhibited by the high nitrogen layer exposed after the TiN layer has failed. This zone appears to be much tougher and intimately bonded (via diffusion gradient) than the TiN layer, with performance characteristics very much like that observed for the low temperature carburizing treatment on 316LN stainless steel [15].

Referring to the exposure time of 1–3 h sonication – after removal of the TiN surface layer as emphasized in Fig. 9 – comparable observations apply to the other nitrided materials, all of which experienced rapid initial weight loss associated with complete removal of the outermost TiN layer on the surface exposed to sonication conditions. For example, the nitrided Ti–6Al–2Sn–4Zr–2Mo alloy performed very similarly to the Ti–6Al–4V material, with a weight loss rate of about 1.5 mg/h for each of the as-received surface and the ground-after-nitriding surfaces, while the residual high nitrogen surface (with just the TiN layer removed) exhibited a weight loss rate of 0.82 mg/h (lowest observed in these experiments). Even after the loss of the TiN layer, the weight loss rate for the residual high nitrogen layer on the Ti–0.12Pd material was decreased by a factor of 2.5 compared to the untreated specimen, and a portion of this "improvement" remained after grinding down to base metal prior to testing due to the higher hardness generated by the nitriding thermal treatment. The weight loss rate for unalloyed Ti was essentially equal for the as-received/mill-annealed specimens and those ground to remove the nitrogen-doped areas, corresponding to similar hardnesses for these two condi-

tions. However, the weight loss rate was somewhat higher for the slightly nitrided surface (exposed by removal of the TiN layer) tested in exposure hours 1–3, suggesting again that increased hardness is not the only factor associated with cavitation–erosion resistance in Hg.

4. Conclusions

Weight loss rates as a function of sonication time in Hg for as-received/mill-annealed and for 20% cold-worked specimens of Ti–6Al–4V and Ti–6Al–2Sn–4Zr–2Mo were approximately equivalent and near 1.25 mg/h. Weight loss rates for unalloyed Ti and Ti–0.12Pd were somewhat higher – by factors of about two and five, respectively – and these specimens suffered non-uniform attack in the form of pitting. Only a slight reduction in weight loss rate was observed as a result of the nitriding treatment selected, but this result was realized only after the outermost TiN surface layer (gold-colored) was eroded from the test surface during the initial minutes of sonication. It is anticipated that this slight improvement in cavitation–erosion resistance is only temporary, as the hardened layer is very thin and its properties (in particular nitrogen concentration, gradient, and bonding characteristics) were not maximized for this service.

The best performing Ti-alloys examined here – Ti–6Al–4V and Ti–6Al–2Sn–4Zr–2Mo – were found to resist pitting damage and exhibit mean (uniform) erosion rates about a factor of three higher than identically tested 316LN stainless steel following a low temperature carburizing treatment. This performance difference is considered minor given that the rate for both materials is very low and manageable (uniform, no/few pits) and represents a through-thickness property for the Ti-alloys as opposed to only a shallow surface property for the carburized stainless steel.

The screening test results for Ti–6Al–4V and Ti–6Al–2Sn–4Zr–2Mo were sufficiently positive that further work to determine the potential suitability of these alloys for target containment associated with potential power upgrades is warranted. More aggressive/prototypic cavitation exposures should be performed, and potential nitriding processes (or other surface modifications) specifically tailored for these Ti-alloy compositions could be investigated in parallel. Similarly, the expected good general corrosion resistance of these alloys in flowing Hg should be confirmed via operation of a thermal convection loop [21] or similar device to examine compatibility at the temperatures and temperature gradients expected during target operation. In addition, data should be gathered to assess potential embrittlement of these alloys in response to the irradiation expected in the SNS spectrum.

Acknowledgements

The authors gratefully acknowledge the contribution of several individuals to this research and report. Funding for the effort was provided through work managed by B.W. Riemer of the Spallation Neutron Source Project at Oak Ridge National Laboratory. A.W. Willoughby performed some of the material acquisition and specimen preparation duties, as well as operated the vibratory horn and aided the post-test evaluation of specimens. H.F. Longmire performed the metallography and microhardness scans on the cavitation buttons, and T.M. Brummett performed the SEM- and macro-photography of test surfaces. E.T. Manneschmidt performed the macro-hardness evaluations. M.P. Brady and G.W. Garner designed and performed, respectively, the nitriding heat treatment described herein. J.R. DiStefano, B.W. Riemer, D.F. Wilson, and B.A. Pint reviewed the report, and F.C. Stooksbury helped prepare the final manuscript.

References

[1] R.P. Taleyarkhan, F. Moraga, C.D. West, in: Proceedings of the Second International Topical Meeting on Nuclear Applications of Accelerator Technology (AccApp98), Gatlinburg, TN, September 1998, p. 650.
[2] F. Moraga, R.P. Taleyarkhan, in: Proceedings of the Third International Topical Meeting on Nuclear Applications of Accelerator Technology (AccApp99), Long Beach, CA, November 1999, p. 301.
[3] R.V. DeMars, M. Siman-Tov, P. Taleyarkhan, et al., in: Transactions of the Amer. Nuc. Soc., vol. 76, June 1997, p. 379.
[4] L.K. Mansur et al., in: Proceedings of the Topical Meeting on Nuclear Applications of Accelerator Technology (AccApp97), Albuquerque, NM, Novemnber 1997, p. 301.
[5] M. Futakawa, H. Kogawa, R. Hino, J. Phys. IV France 10 (2000) Pr9–Pr237.
[6] B.W. Riemer et al., J. Nucl. Mater. 318 (2003) 92.
[7] J.D. Hunn, B.W. Riemer, C.C. Tsai, J. Nucl. Mater. 318 (2003) 102.
[8] K. Kikuchi et al., J. Nucl. Mater. 318 (2003) 84.
[9] J.R. Haines et al., J. Nucl. Mater. 343 (2005) 58.
[10] R. Garcia, F.G. Hammitt, R.E. Nystrom, Erosion by Cavitation or Impingement, ASTM STP 408, American Society for Testing and Materials, 1967, p. 239.
[11] M.D. Kass et al., Tribol. Lett. 5 (1998) 231.
[12] S.G. Young, J.R. Johnston, Erosion by Cavitation or Impingement, ASTM STP 408, American Society for Testing and Materials, 1967, p. 186.
[13] S.J. Pawel, E.T. Manneschmidt, J. Nucl. Mater. 318 (2003) 122.
[14] M. Futakawa et al., J. Nucl. Mater. 343 (2005) 70.
[15] S.J. Pawel, J. Nucl. Mater. 343 (2005) 101.
[16] S.J. Pawel, Assessment of End-of-Life Behavior of the Surface Modification to Improve Cavitation–Erosion Resistance in the Mercury Target at the Spallation Neutron Source, Oak Ridge National Laboratory Technical Memorandum ORNL/TM-2007/063, June 2007.
[17] L.K. Mansur, Oak Ridge National Laboratory Technical Memorandum ORNL/TM-2008/137, Survey of radiation Effects in Titanium Alloys, August 2008.
[18] M.P. Brady et al., JOM, August 2006, p. 50.
[19] Standard Test Method for Cavitation Erosion Using Vibratory Horn Apparatus, ASTM G-32-98, American Society for Testing and Materials, Philadelphia, PA, 1998.
[20] Simoneau et al., in: Proceedings of the 7th International Conference on Erosion by Liquid and Solid Impact, Cambridge, UK, September 1987, p. 32–1.
[21] S.J. Pawel, J.R. DiStefano, E.T. Manneschmidt, J. Nucl. Mater. 296 (2001) 210.